Slow Photoelectron Imaging

Céline Nicole, Ingrid Sluimer, Florentina Rosca-Pruna, Marcel Warntjes, and Marc Vrakking*

FOM Institute for Atomic and Molecular Physics (AMOLF), Kruislaan 407, 1098 SJ Amsterdam, The Netherlands

Christian Bordas

*Laboratoire de Spectrométrie Ionique et Moléculaire, UMR CNRS 5579, Université Claude Bernard,
Lyon 1, Villeurbanne Cedex, France*

Frederic Texier and Francis Robicheaux

Department of Physics, Auburn University, Auburn, Alabama 36849
(Received 24 May 2000)

Experiments are reported on the detection of slow photoelectrons resulting from the photoionization of Xe atoms in a dc electric field by electron imaging. In the far-field photoelectron velocity distributions we can distinguish between direct and indirect ionization processes (involving long range Coulomb interactions with the Xe^+ ion). Also, a new modulation of the velocity distribution is observed which cannot be explained by previously discussed mechanisms. Classical and quantum mechanical calculations are presented to support the interpretations.

Atomic photoionization in the presence of dc electric fields is a playing field for testing classical and quantum mechanical concepts concerning the properties of matter on the microscopic level. In time-dependent wave-packet experiments the preparation of coherent superpositions of electronic states leads to an angular and/or radial localization in the electron wave function and a nontrivial time dependence of the photoionization process [1], while—indirectly—similar information is contained in frequency-domain experiments [2]. In this paper we present for the first time measurements of the asymptotic velocity distribution perpendicular to the dc electric field using an imaging detector [3]. The partitioning of the kinetic energy of the ejected photoelectron between the directions parallel and perpendicular to the field is considerably affected by the Coulomb interaction of the electron with the ion. Thus electrons that ionize directly can be distinguished from electrons that reapproach the atomic core one or more times prior to ionization. While this distinction is supported by a consideration of the classical trajectories in the combined Coulomb and dc fields, a quantum mechanical treatment is needed to analyze interference structures, which are observed here for the first time. Unlike a recent photodetachment experiment [4], the Coulomb interaction causes electrons to oscillate perpendicular to the field, leading to interferences between the corresponding transverse Stark wave functions that manifest themselves in the images.

In the experiments Xe atoms were prepared in the $6s[3/2]_2$ metastable state by using an electron impact source [5] and ionized in an approximately 170 V/cm dc electric field using one- or two-photon ionization employing a tunable linearly polarized dye laser with a bandwidth of 0.08 cm^{-1}. If an atom is placed in a static electric field, photoionization can occur when the atom is excited above the saddle-point energy $E_s = -2\sqrt{F}$. Hence, in the current experiment two-photon ionization was possible at wavelengths ≤651.76 nm. Under our experimental conditions the Stark structure was not resolved and the laser excited an incoherent superposition of Stark and continuum states.

The imaging detector consists of an extraction region containing two electrodes which create the aforementioned electric field and accelerate the electrons into a 50-cm-long field-free time-of-flight tube. The electrons are detected on a 7-cm-diameter microchannel plate (MCP) detector followed by a phosphor screen, which converts electron impacts to light spots which are recorded by a charge-coupled device (CCD) camera. A μ-metal shield surrounds the extraction region and time-of-flight tube.

In electron imaging the kinetic energy and angular distribution are determined by projecting the 3D initial velocity distribution onto a 2D plane perpendicular to the detector axis [6]. It is usually assumed that the ejected electrons interact only with the applied field and follow simple parabolic trajectories. Images are then obtained consisting of rings with a radius proportional to the square root of the kinetic energy and a filling pattern determined by the angular distribution. An important recent advance has been the introduction of velocity map imaging [3]. Here the electron optics design includes a demagnifying lens, which significantly reduces the sensitivity of the detected position to the starting position of the electron, while maintaining the dependence on the electron's initial velocity. Therefore in our setup an ≈100-μm detector resolution was achieved, even though the photoelectron source volume was 1 mm in diameter. This is crucial, since the typical diameter of the images reported in this paper was 1–3 mm.

In the current experiment photoelectron images were recorded for a range of laser wavelengths exciting the atom
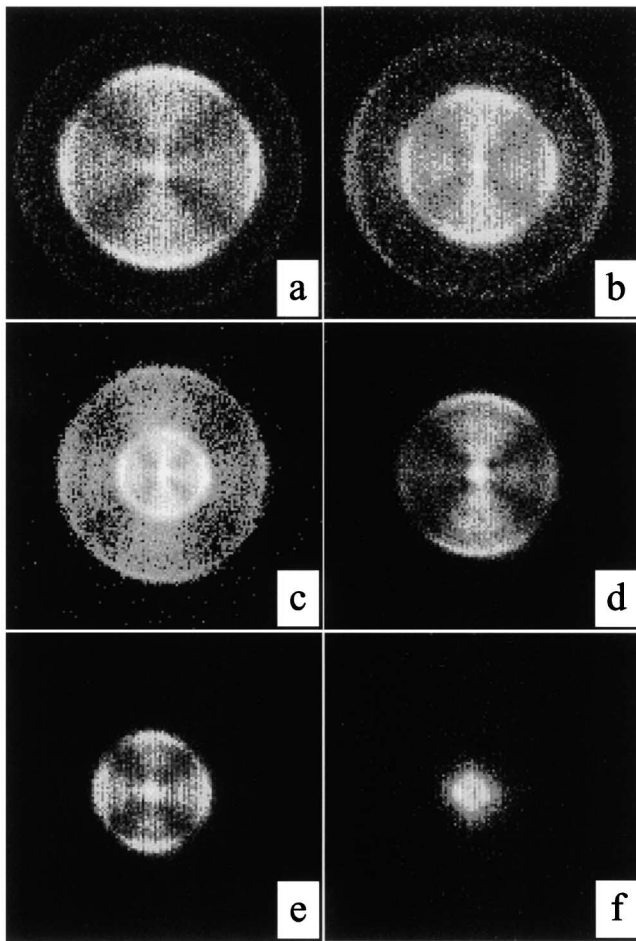
FIG. 1. Photoelectron images recorded for two-photon excitation of Xe($6s[3/2]_2$) in a 170-V/cm dc field with the laser polarization vertical and parallel to the plane of the imaging detector, as a function of the wavelength of the excitation laser: (a) 650.14 nm, (b) 650.40 nm, (c) 650.78 nm, (d) 651.12 nm, (e) 651.42 nm, and (f) 651.68 nm.

close to the saddle point. Figure 1 shows images representative for ionization of Xe by a two-photon transition with the laser polarization parallel to the MCP detector (i.e., perpendicular to the extraction field). A multiple ring structure is clearly visible despite the fact that all photoelectrons are formed with the same initial kinetic energy, in contrast with the single ring structure observed in usual imaging experiments. The angular distribution shows a crosslike structure reflecting the d character in the two-photon ionization process. As the wavelength is scanned changes occur in the radial distributions. The radial distributions are characterized by two main contributions, namely, a primary ring which contracts to a dot as the wavelength is scanned from $\leq$649 to 651.12 nm [Figs. 1(a)–1(d)] and a second ring which becomes prominent around 650.4 nm and which dominates from approximately 651.12 nm [Fig. 1(d)] onwards. This ring contracts to a dot near 651.68 nm [Fig. 1(f)], close to the saddle point. In addition, a dot remains visible in the center of the image for wavelengths $\leq$650 nm. These observations

are qualitatively reproduced for field strengths of 860 and 30 V/cm and when two-photon excitation near 650 nm is replaced by one-photon excitation with light near 325 nm. Furthermore, the radial distributions are not qualitatively affected when the plane of polarization is rotated perpendicular to the screen (parallel to the extraction field).

The results shown in Fig. 1 together with results at additional wavelengths are conveniently collected in a contour plot of the radial distributions as a function of wavelength. This is shown in Fig. 2 for the above-mentioned results using two-photon excitation [Fig. 2(a)], as well as for an experiment using one-photon UV excitation [Fig. 2(b)] with the laser polarization parallel to the detector plane. In both cases, two branches are observed. A difference between Figs. 2(a) and 2(b) is visible around 650.9 nm and is caused by an accidental resonance with the $5d[1/2]_3$ state in the two-photon ionization.

The appearance of two branches in the wavelength dependence of the radial distributions can be explained classically in terms of long range Coulomb interactions of the photoelectron with the Xe^+ ion. The problem of classical motion in a combined Coulomb and Stark field was studied extensively by Kondratovitch and Ostrovsky [7]. Bordas addressed the influence of the Coulomb field on the pattern of impacts of slow electrons on a 2D detector [8]. The key parameter defining the nature of the trajectories is the scaled energy $E^{\#} = E/2\sqrt{F}$, where F is the static electric field strength and E is
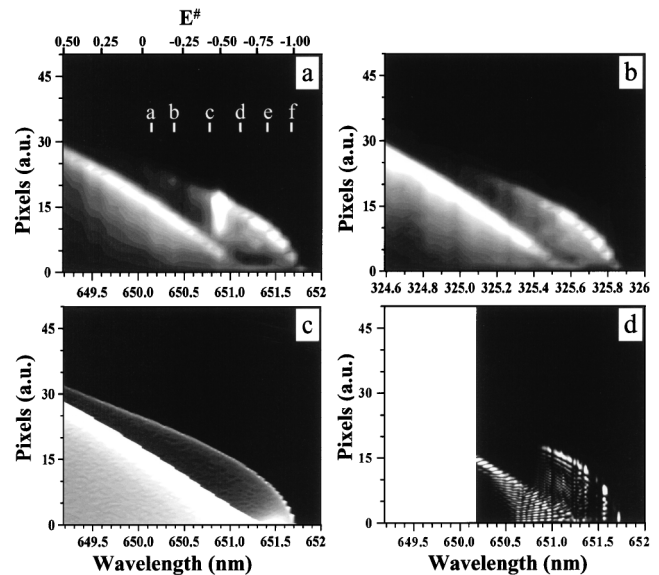

FIG. 2. Contour plots showing experimental and theoretical radial distributions in the photoelectron images as a function of the wavelength for (a) two-photon excitation of Xe($6s[3/2]_2$) with the laser polarization parallel to the plane of the imaging detector (experimental), (b) one-photon excitation of Xe($6s[3/2]_2$) with the laser polarization parallel to the plane of the imaging detector (experimental), (c) a classical hydrogenic model (see text), and (d) a quantum mechanical calculation (see text). Also shown in (a) are the scaled energy and the wavelengths of the measurements shown in Fig. 1. The dc field was 170 V/cm.

the photoelectron energy (with respect to the field-free ionization limit). Classically, photoelectrons fall into three categories, namely, (i) photoelectrons which reach the detector without crossing the detector axis, (ii) photoelectrons which cross the detector axis one or more times, and (iii) photoelectrons which remain bound indefinitely ($E < 0$ only). Fast photoelectrons mostly fall into category (i) [9]. Only electrons initially ejected parallel to the detector axis in the up-field direction pass very close to the Xe^+ ion on the way to the detector and experience a significant deflection from a parabolic trajectory [category (ii)]. For slow photoelectrons the relative importance of categories (ii) and (iii) increases. For $E < 0$ and ejection angles with respect to the field axis $\beta < 2 \arcsin[-E/(2\sqrt{F}\,)]$ the electron does not ionize classically. Next, there is a range of ejection angles such that the photoelectron passes close to the Xe^+ ion one or more times before being detected. Here, the electron motion is strongly affected by the Xe^+ ion and we call this class of trajectories "perturbed." For large ejection angles (i.e., in the down-field direction) the electron motion follows a simple quasiparabolic trajectory and we say that the ionization is direct. Importantly, photoelectrons in categories (i), respectively, (ii), have different asymptotic velocity distributions perpendicular to the field axis. Therefore imaging experiments can distinguish between these two modes of ionization.

In Fig. 2(c) results of classical calculations of the asymptotic velocity distribution for isotropically ejected photoelectrons using the analytical formulas of Refs. [7] and [8] are presented. The two branches are well reproduced. The first branch starting at the saddle point corresponds to electrons which are strongly perturbed by the Coulomb interaction [category (ii)]. The second branch which dominates at lower wavelengths corresponds to electrons which follow quasiparabolic trajectories [category (i)]. The classical theory underestimates the intensity of the branch between 650.94 and 651.6 nm since here a large portion of the trajectories remain bound [category (iii)] whereas excitation above the saddle point in practice always leads to ionization. The classical theory also explains the appearance of a dot in the center of the images at moderate kinetic energies ($1.5 \leq E^{\#} \leq 8$). At the ejection angle separating trajectories falling into categories (i) and (ii) the first axis crossing occurs at the detector and an increased intensity is observed.

A number of observed features are not reproduced classically. For example, Fig. 1(d) clearly shows a radial interference pattern. A series of quantum mechanical calculations were performed based on the method described in Ref. [10], where the details are given for obtaining the outgoing wave functions and dipole matrix elements for multichannel atoms in a static electric field. This method uses zero-field channel coupling matrices and the transformation amplitudes from spherical to parabolic wave functions to obtain the full multichannel wave function in the

field. We calculated all of the zero-field channel coupling matrices for Xe using an R-matrix calculation in LS coupling, while the jj-coupled channel interactions were computed through an LS-jj frame transformation and the K matrices are empirically modified at the few percent level to improve agreement with the zero field, experimental energies. The two-photon dipole matrix elements in zero field were estimated by treating the absorption as only affecting the $6s$ electron in the initial state [11]; errors in the dipole matrix elements dominate all other errors in the calculation.

Besides the spatial degrees of freedom of the electron, there are three other important quantum numbers: J_c—the total angular momentum of the Xe^+ core, Q—the angular momentum that results from coupling the spin of the Rydberg electron to J_c of the core, and M_q—the projection of Q on the z axis. The initial state of Xe can be described as $5p^5 \, ^2P_{3/2} 6s \; J = 2$ with an equal population in each M level and has $J_c = 3/2$, $Q = 2$, $M_q = \pm 2$, ± 1, 0. The calculation uses a coherent superposition of the total M of the final state with an incoherent superposition over each M of the initial state. In our calculation, a very large fraction of the ejected flux leaves the atom in the channel $J_c = 3/2$, $Q = 2$, and M_q the same as the M of the initial state. Thus the Q, M_q quantum numbers are approximately conserved despite all the interactions of the Rydberg electron with the core, which implies the image only weakly depends on the M of the initial state. Hence Xe behaves like an atom with a ^1S core in this experiment, and the images can be qualitatively reproduced by a model without multichannel couplings in zero field.

The full quantum calculations reproduce many nontrivial features of the experiment. The intensity has local maxima in the direction of and orthogonal to the laser polarization. The relative strength of these maxima changes with wavelength and this dependence is accurately reproduced by the calculation. For a spatial resolution exceeding the experiment, the calculation shows that the observed maxima contain a number of fine maxima. Similar to the photodetachment imaging experiment of Ref. [4], these can be related to differences in phase between two or more different paths reaching the same point [12]. The number of fine scale maxima increases with energy above the classical ionization threshold because the semiclassical phase differences between two trajectories increase with energy.

At some wavelengths, the experimental images have clear local maxima as a function of the distance from the center spot. These maxima are reproduced in the calculation [see, for example, Fig. 3 ($\lambda = 651.18$ nm)] and can partly be related to densities of classical trajectories. In Fig. 3 the outermost maximum arises from a singularity in the density of trajectories leaving the nucleus at an angle of $\sim 88°$ with respect to the down-field direction [13]. The central spot mainly arises from electrons ejected at an angle less than $\sim 60°$ from the down-field direction. The origin of the other two maxima (at $\sim \frac{1}{3}$
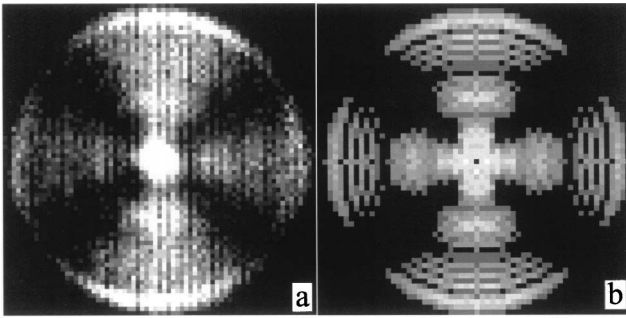
FIG. 3. Comparison between (a) experimental and (b) quantum mechanical results for two-photon excitation of $Xe(6s[3/2]_2)$ in a 170-V/cm field with the laser polarization vertical and parallel to the plane of the imaging detector at a wavelength of 651.18 nm.

and $\sim\frac{2}{3}$ the distance to the outer ring) can be traced to a specific feature of the quantum calculation but apparently does not have a simple classical origin; these two maxima can be reproduced by simply summing the outgoing wave functions that would arise for hydrogen excited in a two-photon transition; the amplitude to reach the point $[\rho = \sqrt{\eta\xi}, z = (\xi - \eta)/2]$ can be approximated by $\alpha(\rho, z) \approx \sum_{n_1} A_{n_1 m} \Xi_{n_1 m}(\xi) \exp[i\phi_{n_1 m}(\eta)]$, where n_1 is the number of nodes in the transverse eigenstate $\Xi_{n_1 m}$ [10], $A_{n_1 m}$ is the amplitude for the electron to be excited to the n_1 channel, and $\phi_{n_1 m}(\eta)$ is the WKB phase in the η coordinate starting from the nucleus where $\eta = 0$ [11]. The large scale modulation requires the interference between several transverse states and complications due to Xe^+ core electrons need not be invoked.

In conclusion, we have shown how direct versus indirect photoionization processes can be recognized using electron imaging, by exploiting the fact that the Coulomb interaction of the electron with the ion alters the asymptotic velocity distribution perpendicular to the electric field. Furthermore, we have found a new modulation in the velocity distribution which does not appear to arise from a classical mechanism or from a simple interference between multiple paths. In the future, these results can be extended in a number of important directions. First, using narrow band lasers individual Stark resonances in the continuum can be excited, allowing the exploration of differences in the ionization dynamics of blue versus red Stark states, where slow photoelectron imaging may allow one to visualize the location of the wave packet. Second, with

novel imaging detectors, allowing time-gated imaging with a tens of picoseconds time resolution, direct and indirect ionization pathways can be studied in wave packets using imaging and time-domain detection simultaneously. Third, slow photoelectron imaging can be applied in nonpurely Coulombic systems such as complex ions and/or cases where an electron interacts with multiple Coulomb centers, as in ZEKE experiments.

*Corresponding author.

[1] G. M. Lankhuijzen and L. D. Noordam, Phys. Rev. Lett. **76**, 1784 (1996).

[2] M. G. Littman, M. L. Zimmerman, T. W. Ducas, R. R. Freeman, and D. Kleppner, Phys. Rev. Lett. **36**, 788 (1976).

[3] A. T. J. Eppink and D. H. Parker, Rev. Sci. Instrum. **68**, 3477 (1997).

[4] C. Blondel, C. Delsart, and F. Dulieu, Phys. Rev. Lett. **77**, 3755 (1996).

[5] A. Kohlhase and S. Kita, Rev. Sci. Instrum. **57**, 2925 (1986).

[6] A. J. R. Heck and D. W. Chandler, Annu. Rev. Phys. Chem. **46**, 335 (1995).

[7] V. D. Kondratovich and V. N. Ostrovsky, Zh. Eksp. Teor. Fiz. **79**, 395 (1980) [Sov. Phys. JETP **52**, 198 (1980)]; J. Phys. B **17**, 1981 (1984); **17**, 2011 (1984); **23**, 21 (1990); **23**, 3785 (1990).

[8] Ch. Bordas, Phys. Rev. A **58**, 400 (1998).

[9] For example, for $E^\# = 2$, 97% of the trajectories reach the detector without crossing the detector axis.

[10] F. Robicheaux, C. Wesdorp, and L. D. Noordam, Phys. Rev. A **60**, 1420 (1999).

[11] The details of the quantum formulation and the calculation of zero-field channel couplings will be described at a later date.

[12] For example, there are roughly 40 rings at $\lambda = 651$ nm.

[13] Another singularity at an angle $\sim29°$ gives a maximum in the quantum calculation within the central probability of the experiment.